SAND2019-14608C

Digital Phase-Sensitive Holography for Numerical Shock-wave Distortion Cancellation

Tyrus M. Evans*, Andrew W. Marsh†, Jaylon Uzodinma‡, and Yi Chen Mazumdar §
Georgia Institute of Technology, Atlanta, GA, 30332, USA

Daniel R. Guildenbecher¶
Sandia National Laboratories, Albuquerque, NM, 87185, USA

In extreme supersonic, hypersonic, or explosive environments, the presence of gas-phase shocks cause coherent imaging distortions and inhibit object tracking. In this work, we aim to remove these distortions by measuring the relative phase of the light using digital phase-sensitive holography techniques including a two-step phase-shifting technique and a single-shot polarization phase-shifting technique. Once the phase of the shock-wave is acquired, the distortion is numerically canceled from the image and the un-distorted object image is recovered. This work discusses the theory, provides simulation results, and presents preliminary experimental data showing how this concept can be applied to remove shock-wave phase distortions created by supersonic air jets.

I. Introduction

Digital holography includes a class of quantitative techniques [1, 2] for object sizing and three-dimensional object tracking in multiphase flows [3–9] and combustion systems [10–13]. As the conditions become more extreme in supersonic, hypersonic, or explosive environments [14], however, the shock-waves and other density gradients begin to distort coherent images, as illustrated in Fig. 1. This, in turn, makes it more difficult to image objects of interests, such as droplets, particles, explosively generated fragments, or other objects.

One interesting technique that has been applied to remove these distortions is phase-conjugate digital in-line holography (PCDIH) [15–17]. In this technique, the imaging beam is passed through the object, shock-wave distortion, and a phase-conjugate (PC) mirror. The PC mirror reflects light with the conjugate phase. When this light passes back through the shock-wave distortion, the phases cancel and the distortion is significantly reduced. The minor distortions that remain in the image are associated with light refraction from the edges of the shock-wave and the shock-wave motion during the laser light time-of-flight back and forth from the PC mirror [16]. Although PCDIH works well for single-shot *in situ* phase distortion cancellation, it has a high degree of complexity, utilizes nonlinear four-wave-mixing phenomena, requires high laser energies, and is difficult to scale to ultra-high repetition rates [16]. Therefore, alternative techniques need to be explored for phase distortion cancellation.

One possible approach for phase distortion cancellation is to measure the phase directly and then *numerically cancel* the distortion. There are several existing methods for measuring phase with holography; these are typically used for microscopy or for examining biological systems. One method for measuring phase is the angular spectrum method, which uses filtering of the angular spectrum to measure and reconstruct the amplitude and phase numerically [18]. Han et al. [19], utilize a different two-step phase-shifting method that requires four interferograms recorded sequentially on two cameras to calculate phase for image reconstruction. While this method and other similar methods work well on stationary objects [20, 21], they are ill-suited for high-speed applications. A separate class of parallel phase-shifting techniques or polarization phase-shifting techniques [22–30], utilize a single polarization-imaging camera to record several holograms at different polarizations simultaneously. Phase-shifting algorithms are then used to construct the amplitude and phase. In addition, it is also possible to collect phase information by tilting the reference beam with respect to the object beam (off-axis configuration [31–36]) to generate tight interference fringes. Separate images with different phases are then generated from different locations within in the interference fringes. While these techniques

*Undergraduate Researcher, Guggenheim School of Aerospace Engineering, tyrusevans@gatech.edu.
†Ph.D. Candidate, Woodruff School of Mechanical Engineering.
‡Summer Undergraduate Researcher, Woodruff School of Mechanical Engineering, juzodinma3@gatech.edu.
§Assistant Professor, Woodruff School of Mechanical Engineering, ellen.mazumdar@me.gatech.edu, Member AIAA.
¶Principal Member of the Technical Staff, Engineering Sciences Center, drguild@sandia.gov, Member AIAA.

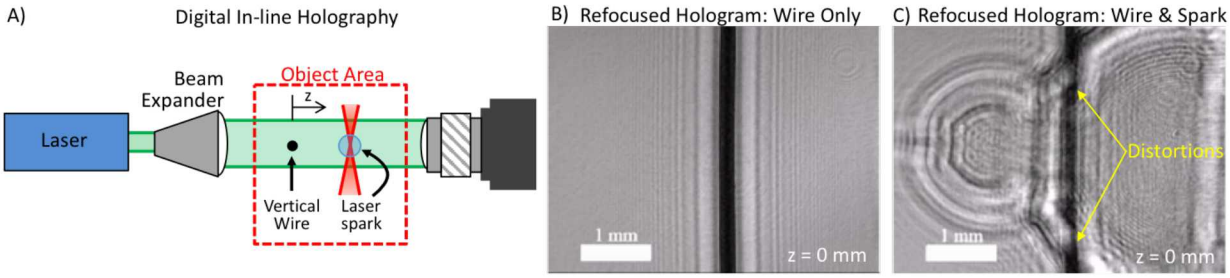

Fig. 1 Shock-waves and other phase distortions in coherent imaging applications, like digital in-line holography, tend to distort images of absorptive objects. A) In the simplified setup, B) the refocused hologram of a vertical wire (only the wire is shown) can be C) distorted by a laser-spark plasma-generated shock-wave [15].

provide methods for measuring phase, there has been little work on utilizing the phase measurements for numerical distortion cancellation. Sánchez-Ortiga et al. [37], for example, utilize a pure-optical phase canceling technique with a telecentric lens architecture. However, this type of technique used to cancel known imaging system distortions cannot be used to cancel shock-wave phase distortions that can change from test to test.

The digital phase-sensitive holography techniques described earlier have a few advantages over PCDIH approaches. First, high laser energies are not needed, since digital phase-sensitive holography utilizes linear optical phenomena. Therefore, the measurement techniques tend to be more scalable for multiple views and ultra-high repetition rates. Second, direct phase measurements enable estimation of density distributions inside a shock-wave. Digital phase-sensitive holography, however, also has several disadvantages including high precision positioning requirements, image registration requirements across multiple cameras, or image interpolation requirements when using a polarization camera. PCDIH is inherently an *in situ* technique, which means that successful distortion cancellation can be viewed immediately but also means that there will be significant laser-light time-of-flight effects. Phase holography does not suffer from laser-light time-of-flight effects, which can potentially lead to more complete distortion cancellation.

In this work, we outline the theoretical foundations for phase-sensitive holography techniques and demonstrate simulations that show how phase disturbances can be numerically cancelled. Different topologies including a two-step phase-shifting technique and a single-shot polarization phase-shifting technique are discussed. The techniques are compared with the aim of achieving digital phase distortion cancellation with a single laser shot, minimizing setup complexity, and increasing phase measurement signal-to-noise. Finally, experiments are conducted to illustrate application of digital phase-sensitive holography for the removal of phase distortions generated by supersonic air jets.

II. Digital In-line Holography

A. Propagation and Refocusing

In digital in-line holography (DIH), a reference laser beam with an electric field of $R(x,y) = A_r(x,y)e^{ikz-i\omega t}$ is passed through a field containing amplitude or phase objects of interest. Here, $k = 2\pi/\lambda$ is the wavenumber, λ is the wavelength, and ω is the frequency. Each object has a transmission function $t(x,y) = e^{-a(x,y)+i\phi(x,y)}$ with absorption $a(x,y)$ and phase $\phi(x,y)$ properties. When the light diffracts off of the particles forming the object wave, the propagation of light follows the Fresnel-Kirchhoff diffraction function [38] that can be approximated as,

$$O(x,y,z) = (R(x,y) \cdot t(x,y)) \otimes g_f(x,y,z). \tag{1}$$

Here, $\otimes$ is the convolution operator, $g_f = FT^{-1}(G)$, and G is the kernel defined in Eq.(8). The electric field of light contains both amplitude and phase information. However, the electric field cannot be directly measured. The intensity of the interference pattern $I_c(x,y) = |O(x,y,z_c)|^2$ representing the raw hologram collected downstream at z_c, however, can be measured with a digital in-line holography topology [1, 2]. In DIH, the intensity images can be numerically refocused in z to produce three-dimensional holograms from two-dimensional raw images using,

$$E_h(x,y,z) = [I_c(x,y)R^*(x,y)] \otimes g_b(x,y,z), \tag{2}$$

where E_h is the reconstructed amplitude, $R^*(x,y)$ is the planar conjugate reference wave, and $g_b = FT^{-1}(G^*)$. The refocused images can then be visualized using the amplitude $A_h = |E_h|$. While E_h is complex, it does not provide a

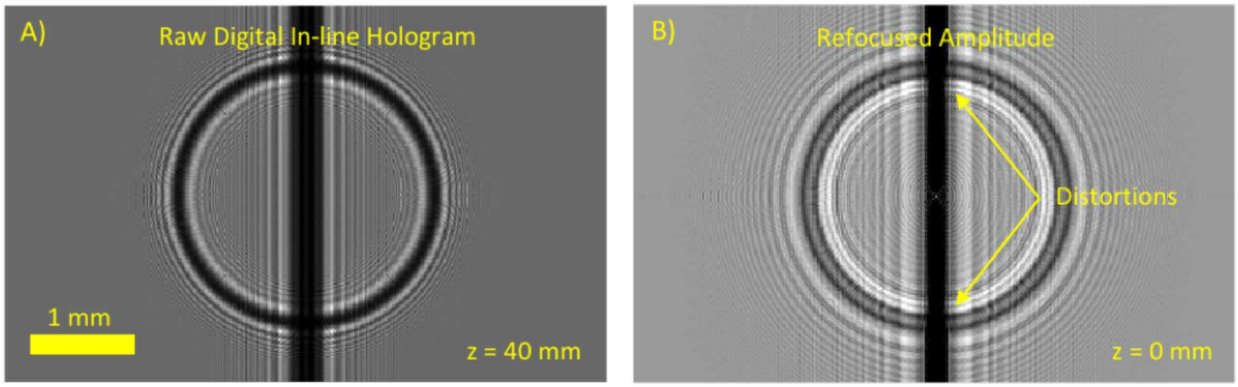

Fig. 2 Simulated results utilizing traditional digital in-line holography algorithms (Eq.(2)) are demonstrated. A) The raw intensity hologram taken at the camera imaging plane and B) the numerically refocused image at the wire image plane showing shock-wave distortions are illustrated. The simulation contains a wire at z = 0 mm, spherical shock-wave at z = 20 mm, and camera at z = 40 mm.

true reconstruction of $O(x, y, z)$ because it contains symmetric twin holograms at $+z$ and $-z$ and does not preserve the original phase information from the object wave.

The z-location of each absorptive or scattering object can be found when edges come into focus. Numerically, this can be done by optimizing a focus metric that minimizes amplitude and maximizes edge sharpness [39]. Additional algorithms can then be used to determine particle size, improve dynamic range, track particle velocity, and correct biases [40–42]. Overlapping objects are very difficult to quantify as the diffraction patterns from one object will tend to obscure the diffraction patterns from another object. In these cases, multiple imaging beams [8, 43] can potentially be used. If a phase object overlaps with an absorptive object, however, the phase delays will severely distort the edges of the absorptive object making it difficult to determine the shape and z-depth [15]. Thus, when working with both phase and amplitude objects, alternative numerical techniques are needed.

B. Digital In-line Holography Simulations

For the initial simulations, a vertical wire and a spherical shock-wave generated by a laser spark are utilized as the amplitude and phase object, respectively [16, 38]. The former is created as a thin wire and the latter is created as a constant-density spherical shock-wave phase distortion (generated as a phase disk located at a single fixed z-plane surrounded by light refraction at the edges, which is modeled as absorption), both placed at different distances from the camera. Here, the wire is located at $z = 0$ mm, the shock-wave is located at $z = 20$ mm, and the camera located at $z = 40$ mm. The MATLAB simulations for the raw hologram captured at the camera plane is illustrated Fig. 2. When the raw hologram is numerically refocused via traditional DIH algorithms using Eq.(2) to the wire image plane, as shown in the right-most image of Fig. 2, some distortion of the wire can be seen along with the out-of-focus spherical shock-wave phase distortion. From this set of images, it is clear that traditional DIH algorithms cannot be used to separate the contributions of the shock-wave from the wire. This simulated configuration, however, serves as an excellent test-case for alternative numerical phase cancellation techniques and allows results of different techniques to be compared.

III. Two-step Phase-shifting Digital Phase Holography

One promising technique for measuring phase distortions is a two-step phase-shifting method originally proposed by Han et al. for cell microscopy [19]. In this method, two separate cameras at different z-positions are used to capture two images each at different phase shifts (four images total). Using this method, it is possible to reconstruct the electric field of the original object wave, and thus extract the phase contributed by the shock-wave distortion. Because the original method requires two images per camera, it is ill-suited for single-shot applications. However, it can be expanded for use on stationary phase distortions, such as stationary shock-waves. Alternatively, it can also be modified into a single-shot four-image technique. This can be implemented using four cameras or by mapping four holograms onto the same camera.

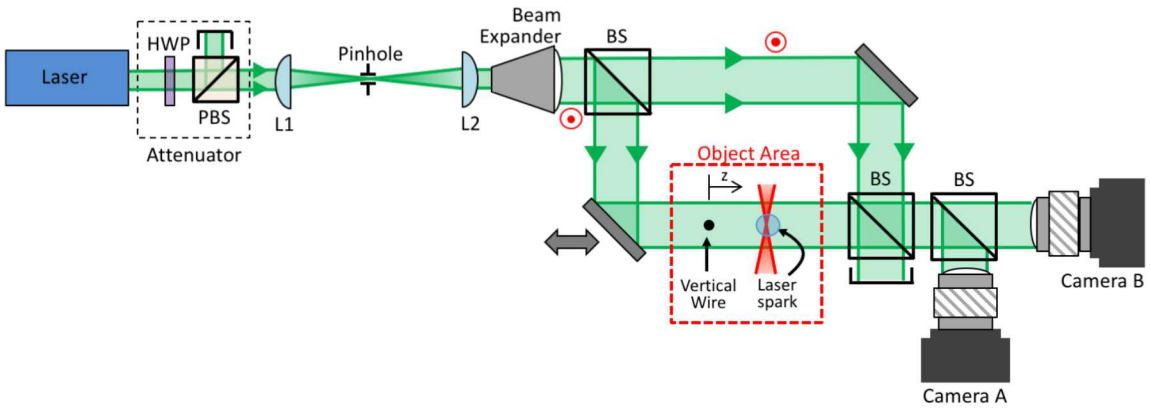

Fig. 3 Experimental setup for the two-step phase-shifting method is shown. (HWP–half wave plate; PBS–polarizing beam splitter; L1–50 mm focal length lens; L2–400 mm focal length lens; BS–beam splitter)

A. Experimental Setup

A two-camera, two-step phase-shifting setup is illustrated in Fig. 3. In this arrangement, 532 nm coherent laser light is passed through an attenuator to control the intensity and polarization. Then the beam is spatially filtered, expanded, and collimated into a Mach-Zehnder interferometer. One of the legs of the interferometer is used as the reference beam while the other leg contains the object area, where a variety of phase distortions can be measured. With this arrangement, two pictures must be captured by each camera, camera A and camera B. For the two-step phase-shifting method, the image planes for the two cameras need to be placed at different distances from the vertical wire and shock-wave. This can be done by adjusting the camera lens focus or by physically shifting the camera z-location for lens-less implementations.

B. Simulation Results

To calculate the phase disturbance from the collected holograms, a two-step phase-shifting numerical algorithm [19] is implemented. In this method, four interferograms represented by Eqs.(3), (4), (5), and (6) are implemented as,

$$I_{1a}(x,y,z_1) = |O(x,y,z_1)|^2 + |R|^2 + (O(x,y,z_1))\,R^* + (O_{z1}{}^*)\,R, \tag{3}$$

$$I_{1b}(x,y,z_1) = |O(x,y,z_1)|^2 + |R|^2 - (O(x,y,z_1))\,R^* - (O_{z1}{}^*)\,R, \tag{4}$$

$$I_{2a}(x,y,z_2) = |O(x,y,z_2)|^2 + |R|^2 + (O(x,y,z_2))\,R^* + (O_{z2}{}^*)\,R, \tag{5}$$

$$I_{2b}(x,y,z_2) = |O(x,y,z_2)|^2 + |R|^2 - (O(x,y,z_2))\,R^* - (O_{z2}{}^*)\,R. \tag{6}$$

The first two equations represent images taken with camera A at distance z_1 from the camera to the shock-wave using different π-phase shifts. The second two equations represent images taken with camera B at distance z_2 using different π-phase shifts. In the case of simulations done in this work, the object wave O is the same as the one shown previously in the DIH simulations prior to conversion to intensity (Fig. 2). The intensities of these four interferograms are shown in Fig. 4. Next, the original object wave at the shock-wave plane is estimated using Eq. (7) and the diffraction kernel in Eq.(8) such that,

$$FT\{\hat{O}(x,y,z_s)\} = \frac{FT\{I_{2a}-I_{2b}\}G(-z_1) - FT\{I_{1a}-I_{1b}\}G(-z_2)}{2(G(z_2-z_1)-G(z_1-z_2))}, \tag{7}$$

$$G(z) = e^{(2\pi i z/\lambda)\sqrt{1-(\lambda u)^2-(\lambda v)^2}}. \tag{8}$$

Here, u and v represent spatial coordinates in the frequency domain. By taking an inverse Fourier transform of Eq. (7), the original object wave can be calculated containing the amplitude and phase components located at the shock-wave plane z_s. The reconstructed object image at the wire-plane and the calculated phase for $\hat{O}$ at the shock-wave plane are shown in Fig. 5. The figure on the left shows the in-focus shock-wave edges and the out-of-focus wire. The right image shows the phase measurement at the shock-wave plane. With additional numerical processing and advanced phase unwrapping techniques, it is possible to use this method for phase measurements of the density gradient in the shock-wave.

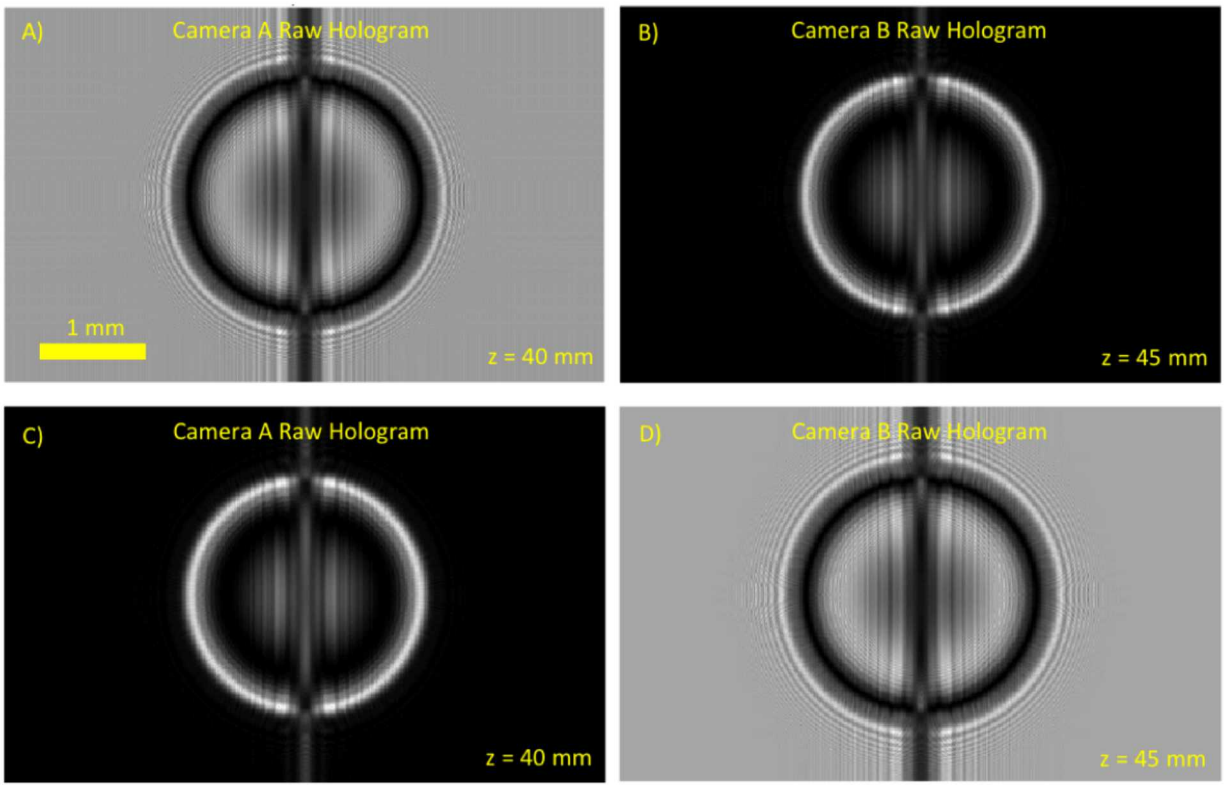

Fig. 4 Four simulated interferograms collected via the two-step phase-shifting method are illustrated. Interferograms A) and C) are collected at a distance of z = 40 mm (z_1 = 20 mm) using camera A and are shifted from each other by a factor of π. Interferograms B) and D) are collected at a distance of z = 45 mm (z_2 = 25 mm) using camera B and are also shifted by a factor of π from each other.

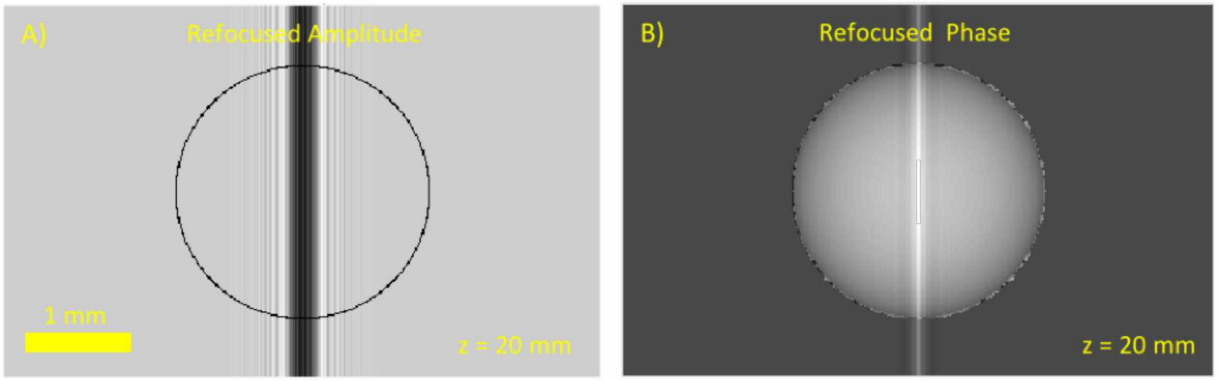

Fig. 5 A) Numerically refocused hologram from the two-step phase-shifting simulations using $\hat{O}$ at z = 20 mm is shown. B) On the right is the numerically refocused simulated phase distribution of the object wave $\hat{O}$ at z = 20 mm.

IV. Single-Shot Polarization Phase-Shifting

Another method for capturing the phase uses the single-shot polarization (parallel) phase-shifting technique, which involves collecting multiple interferograms simultaneously from a single polarization camera [23]. This technique is easier to apply in high-speed environments where objects or phase distortions move quickly. Polarization phase-shifting digital holography has been used to obtain time-resolved images of compressed gas flow [23], which indicates its

potential for dynamic shock wave imaging. In this technique, a polarization-imaging camera is used to record multiple holograms simultaneously. The holograms are extracted from the camera and interpolated before phase-shifting algorithms are used to reconstruct the object wave.

A. Experimental Setup

An experimental setup which utilizes a polarization camera for phase-sensitive digital holography is shown in Fig. 6. Similar to the setup shown in Fig. 3, 532 nm coherent light is passed through an attenuator to control intensity and polarization. This beam is also spatially filtered, expanded and collimated into a Mach-Zehnder interferometer. One leg (reference beam) of the inferometer is passed through a half wave plate, while the other leg (object beam) passes through the object area containing a wire and a stationary air jet. By passing the reference beam through a half wave plate, a $\pi/2$ phase shift is generated. The object and reference beams then recombine and pass through a quarter wave plate to induce a $\pi/4$ phase shift, producing clockwise and counterclockwise polarizations. The polarization camera, which has alternating pixels with different polarization orientations, captures four inter-laced holograms with four different phases.

B. Simulation Results

To reconstruct the object wave, a parallel phase-shifting numerical algorithm is used. Similar to the two-step phase-shifting numerical algorithm, this method requires four interferograms represented by Eqs.(9), (10), (11), and (12). Here, the intensity at each pixel can be calculated as,

$$I_0(x,y,z_c) = |O(x,y,z)\cdot e^{i\cdot 0} + R|^2, \tag{9}$$

$$I_{\frac{\pi}{2}}(x,y,z_c) = |O(x,y,z)\cdot e^{i\cdot \frac{\pi}{2}} + R|^2, \tag{10}$$

$$I_{\pi}(x,y,z_c) = |O(x,y,z)\cdot e^{i\cdot \pi} + R|^2, \tag{11}$$

$$I_{\frac{3\pi}{2}}(x,y,z_c) = |O(x,y,z)\cdot e^{i\cdot \frac{3\pi}{2}} + R|^2, \tag{12}$$

where z_c is the image plane of the camera. Each of these interferograms represents an intensity image separated by a phase shift of $\frac{\pi}{2}$, as simulated in Fig. 7. The interferograms are comprised of the sum of the original object image with the phase shift and a reference beam. Individually, each interferogram only contains intensity information from the object wave. However, using all four interferograms, the reconstructed object wave can be found using Eq. (13),

$$\widetilde{O}(x,y,z_c) = (I_0 - I_\pi) - i\left(I_{\frac{\pi}{2}} - I_{\frac{3\pi}{2}}\right). \tag{13}$$

The resulting reconstructed object wave ($\widetilde{O}$) now contains both the intensity data and the phase data of the hologram. While the object wave can be reconstructed using fewer than four images [28, 29], these alternative techniques require

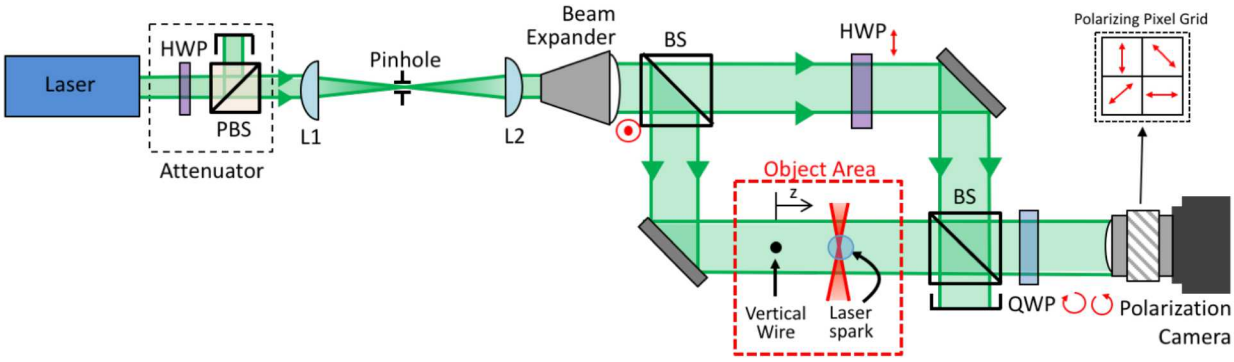

Fig. 6 Experimental setup for the single-shot polarization phase-shifting method is shown with a polarization camera. Images are taken with a pixel array with alternating polarization orientations as seen above. (HWP–half wave plate; QWP–quarter wave plane; PBS–polarizing beam splitter; L1–50 mm focal length lens; L2–400 mm focal length lens; BS–beam splitter)

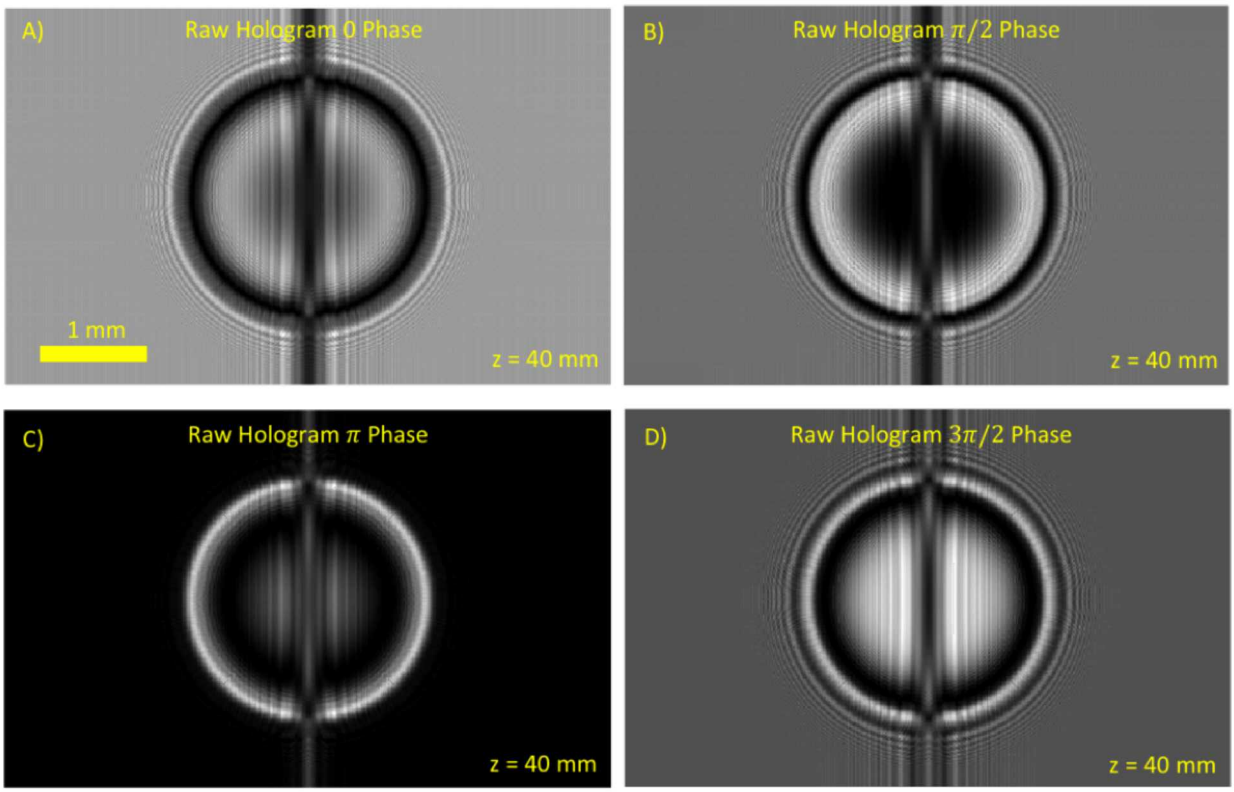

Fig. 7 Four simulated interferograms collected via the single-shot polarization phase-shifting method are illustrated. Each interferogram is a raw simulation image taken at the camera imaging plane (z_c = 40 mm). Each interferogram is separated by a phase shift of $\frac{\pi}{2}$ and governed by Eqs.(9), (10), (11), and (12).

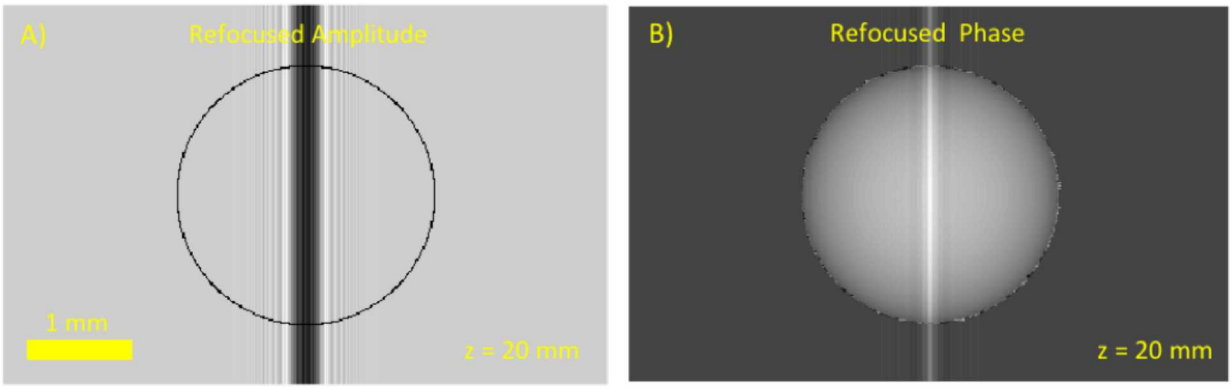

Fig. 8 Numerically refocused images from the single-shot polarization phase-shifting simulations using Eqs. (13) and (14) are illustrated. The image on the left shows the in-focus shock-wave edge as well as the out-of-focus wire (z = 20 mm). The image on the right shows the measured phase of the shock-wave and the phase contributions of the out-of-focus wire (z = 20mm).

more complex relatively intensity calibrations. In this technique, the phase of the object wave collected at the camera image plane can be calculated by using,

$$\widetilde{\phi}(x, y, z_c) = tan^{-1}\left(\frac{I_0 - I_\pi}{I_{\frac{\pi}{2}} - I_{\frac{3\pi}{2}}}\right). \tag{14}$$

In Fig. 8, the image on the left shows an out-of-focus vertical wire and an in-focus circle representing light loss due to refraction from the shock-wave edges. In this plane (which can be determined by finding where the shock-wave edges come into focus) the phase distortions only exist in the phase image and not in the amplitude image. However, if we were to propagate forward or backward away from this plane, the phase distortions would propagate into the amplitude images, which is the root cause of the distortions. The phase shown in the right image of Fig. 8 contains both the circular phase disk and the phase generated by the out-of-focus wire. In the future, the phase contributions of the wire can potentially be removed to show only the contribution of pure phase objects, like shock-waves or density gradients in the air. While the mathematical process used to generate the object wave in this example is different from the two-step phase-shifting procedure, the resulting amplitude and phase are similar.

V. Phase Cancellation via Conjugate Multiplication

While previous work has focused on quantifying the phase disturbances in holograms, little effort has been made to cancel these phase distortions in a extreme environments. Using the reconstructed object waves from the two techniques discussed above, both phase and amplitude data is now available. Because phase data is retained (and not lost in the case of absorption), phase cancellation is possible if the object wave is known.

One method for phase cancellation utilizes conjugate multiplication. In this technique, the electric field is numerically refocused to the center of the shock-wave plane, where it is multiplied by its conjugate, as shown in Eq. (15). This technique and other similar methods do not require the user to know the shape or density distribution in the shock-wave, only the location of the shock-wave plane (typically located where the shock-wave edge comes into focus) needs to be known. The resulting electric field contains a constant phase at the plane of the shock-wave distortion such that,

$$O_{NP} = O^* \cdot O, \tag{15}$$

where O_{NP} is the object hologram without any phase disturbance and the object wave O derived from any technique can be used ($\hat{O}$ or $\widetilde{O}$). Once these phase distortions are removed from the shock-wave plane via cancellation, they will not propagate distortions to the wire plane, which then produces undistorted wire images.

The conjugate multiplication process illustrated in in Eq. (16) shows how the the transmission function of the reconstructed object hologram $t(x,y) = e^{-a(x,y)+i\phi(x,y)}$ and its conjugate can be combined into a new transmission function containing twice the absorption and no phase elements,

$$t_{NP}(x,y) = e^{-a(x,y)-i\phi(x,y)} \cdot e^{-a(x,y)+i\phi(x,y)} = e^{-2a(x,y)}. \tag{16}$$

This result is similar to the physical processes occurring in PCDIH [16] where the conjugate wave passes back through the distortions. In the case of PCDIH, passing the beam back through the object area doubles the absorption losses but removing any phase disturbances. However, in this numerical distortion removal process, a single-shot image can be taken to replicate this process without any time-of-flight delays.

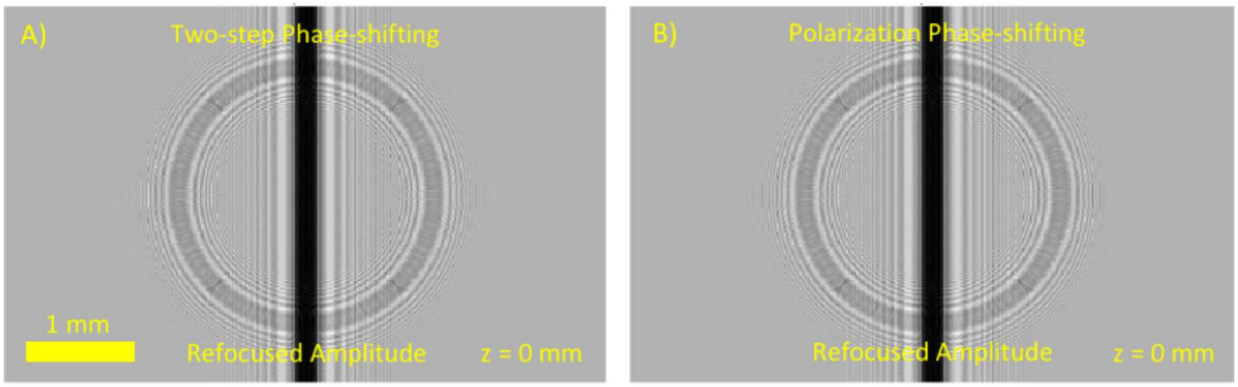

Fig. 9 Simulated holograms are refocused to the wire focal plane. This data shows successful distortion cancellation from data gathered using A) the two-step phase-shifting method and B) the polarization phase-shifting method.

While this method for distortion cancellation is simple, it assumes that the phase distortion can be approximated as located in a single plane. Additionally, it also removes some phase contributions from the wire, which is undesirable. For more complex shock-wave and object configurations, more advanced alternative methods for calculating and correcting the object wave should be used. Nevertheless, the reconstructed images showing successful shock-wave distortion removal via phase-sensitive hologram acquisition (two-step phase-shifting and polarization phase-shifting) and conjugate multiplication are shown in Fig. 9. No phase distortions from the shock-waves can be seen on the wires in this figure, which is a direct contrast to Fig. 2B. The visible rings from losses at the shock-wave edges (modeled as absorption), however, are still visible. Although the implementation of the two phase-shifting methods differ, the final phase-distortion-cancelled images are similar.

VI. Experimental Results

Preliminary digital phase-sensitive holography experiments were conducted by imaging a vertical wire through an underexpanded supersonic air jet produced by a 1.5 mm (design Mach number = 1) nozzle at 90 psig. The single-shot polarization phase-shifting experimental setup shown in Fig. 6 was used for this experiment because it is less sensitive

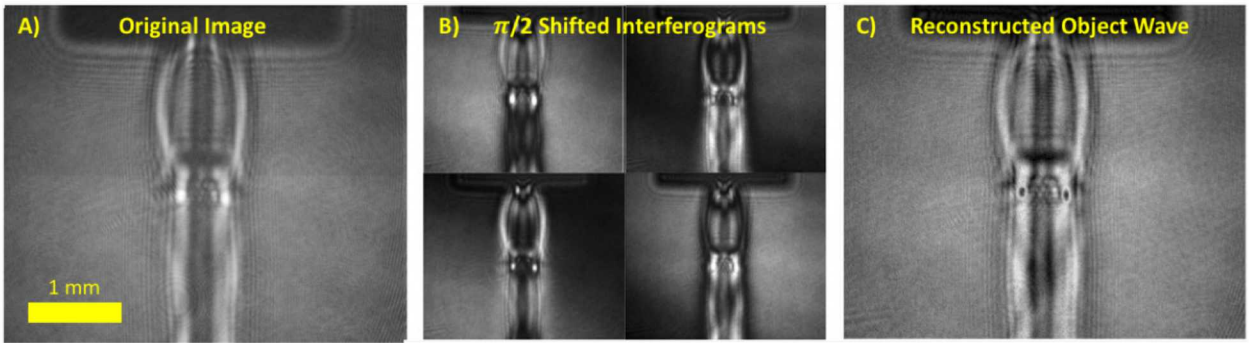

Fig. 10 A) The raw hologram of a vertical wire with a stationary shock-wave distortion in front as collected by a polarization camera is shown. B) The four interferograms at 0, $\pi/2$, π, and $3\pi/2$ that are obtained through cubic interpolation of the original raw image are also illustrated. C) This is used to reconstruct the object wave using Eq. 13 and is shown as an amplitude image.

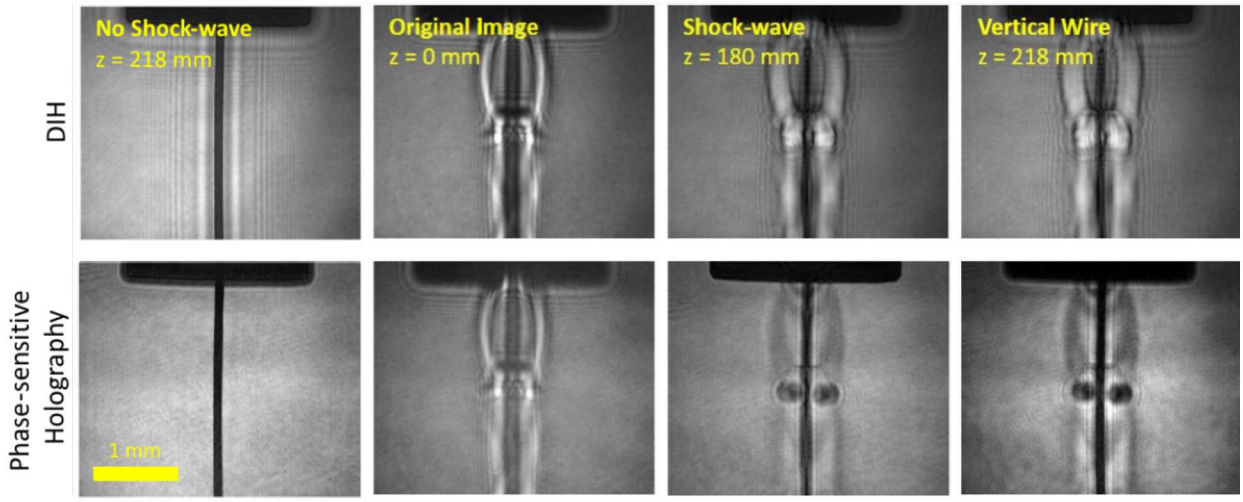

Fig. 11 Numerical refocusing is illustrated using DIH (top) and phase-sensitive holography (bottom). The DIH images at both the shock-wave and wire plane appear significantly distorted while the phase-sensitive holography images that were corrected using conjugate multiplication appear distortion-free in both the shock-wave plane (Mach disk is visible) and the wire plane (wire edges are un-distorted).

to misalignment (requires less precision) and can be captured with a single shot. Using a 532 nm continuous wave laser, single-shot images were captured with a FLIR Blackfly S Polarization Camera (pixel pitch of 3.45 μm) with an exposure of 72 μs. The camera has four-directional polarizers that splits a group of four pixels into grids with four different $\pi/2$ phase shifts, as shown in Fig. 6. To compile the interferograms seen in Fig. 10B, all the pixels from a specific polarized state are grouped together. The missing pixels in between are filled in using two dimensional cubic interpolation [23]. Using the reconstruction method outlined in Eq. 13, the electric field in Fig. 10C containing both intensity and phase information is calculated. Applying conjugate multiplication phase correction to the reconstructed field at the center of the Mach cone yielded the distortion-free vertical wire in the bottom row of Fig. 11.

In order to determine the effectiveness of the distortion removal technique, DIH images in Fig. 11 were acquired for comparison. The DIH images were captured by blocking the reference beam, only allowing the object beam to reach the camera (DIH is a self-referencing technique). Refocusing the hologram to the wire location reveals a distorted wire edge where the shock-wave distortion intersects, as shown in Figure 11. From initial qualitative analysis, the edge of the wire for the DIH images appear significantly more distorted than that of the images where conjugate multiplication phase correction was applied. The images obtained through phase-sensitive holography also have the distinct advantage over DIH of having a clear, in-focus shock-wave edge (Mach disk is clearly visible) when the image is propagated to the shock-wave image plane, as shown in Figure 11.

VII. Conclusion

In this paper, phase-sensitive holography techniques were explored as a method for numerical phase distortion removal. By using $\pi/2$ shifted interferograms, the electric field containing both intensity and phase data was found. By propagating the electric field to the shock-wave distortion plane and applying conjugate multiplication, the phase distortions were effectively canceled. This distortion correction method was effectively applied to simulations for polarization (parallel) and two-step phase-shifting topologies. Preliminary experimental results gathered using a polarization (parallel) phase-shifting experimental setup and a polarization camera showed the ability to numerically remove the distortions cause by a stationary supersonic shock-wave. Conjugate multiplication was applied at the shock-wave plane to generate these results.

This technique has the potential to open avenues for three-dimensional tracking of supersonic multi-phase flows without the use of a complicated and expensive PCDIH setup. This is especially applicable to supersonic, hypersonic, and explosive environments. Ultimately, further experimental results in more extreme conditions are needed to determine the advantages and disadvantages of this numerical distortion removal technique.

Acknowledgments

The authors would like to thank the Laboratory Directed Research and Development program at Sandia National Laboratories, which is a multimission laboratory managed and operated by National Technology and Engineering Solutions of Sandia, LLC., a wholly owned subsidiary of Honeywell International, Inc., for the U.S. Department of Energy's National Nuclear Security Administration under contract DE-NA0003525.

References

[1] Gabor, D. A., "New Microscopic Principle," *Nature*, Vol. 161, 1948, pp. 777–778.

[2] Schnars, U., and Jueptner, W., *Digital Holography: Digital Hologram Recording, Numerical Reconstruction, and Related Techniques*, Springer, 2005.

[3] Chen, Y., Wagner, J. L., Farias, P. A., DeMauro, E. P., and Guildenbecher, D. R., "Galinstan Liquid Metal Breakup and Droplet Formation in a Shock-induced Cross-flow," *Int. J. Multiphase Flow*, Vol. 106, 2018, pp. 147–163.

[4] Guildenbecher, D. R., Wagner, J. L., Olles, J. D., Chen, Y., DeMauro, E. P., Farias, P. A., Grasser, T. W., and Sojka, P. E., "kHz Rate Digital In-Line Holography Applied to Quantify Secondary Droplets from the Aerodynamic Breakup of a Liquid Column in a Shock-Tube," *54th AIAA Aerospace Sciences Meeting, AIAA SciTech*, 2016. AIAA-2016-1044.

[5] Chen, Y., Wagner, J. L., Farias, P. A., and Guildenbecher, D. R., "Study of Galinstan Liquid Metal Breakup Using Backlit Imaging and Digital In-line Holography," *14th International Conference on Liquid Atomization and Spray Systems (ICLASS)*, 2018.

[6] Katz, J., and Sheng, J., "Applications of Holography in Fluid Mechanics and Particle Dynamics," *Annu. Rev. Fluid Mech.*, Vol. 42, 2010, pp. 531–555.

[7] Sheng, J., Malkiel, E., and Katz, J., "Single Beam Two-views Holographic Particle Image Velocimetry," *Appl. Opt.*, Vol. 42, No. 2, 2003, pp. 235–250.

[8] Sheng, J., Malkiel, E., and Katz, J., "Digital Holographic Microscope for Measuring Three-dimensional Particle Distributions and Motions," *Appl. Opt.*, Vol. 45, 2006, pp. 3893–3901.

[9] Sheng, J., Malkiel, E., and Katz, J., "Using Digital Holographic Microscopy for Simultaneous Measurements of 3D Near Wall Velocity and Wall Shear Stress in a Turbulent Boundary Layer," *Exp. Fluids*, Vol. 45, 2008, pp. 1023–1035.

[10] Chen, Y., Guildenbecher, D. R., Hoffmeister, K. N. G., Cooper, M. A., Stauffacher, H. L., Oliver, M. S., and Washburn, E. B., "Study of Aluminum Particle Combustion in Solid Propellant Plumes using Digital In-line Holography and Imaging Pyrometry," *Combust. Flame*, Vol. 182C, 2017, pp. 225–237.

[11] Powell, M. S., Gunduz, I. W., Shang, W., Chen, J., Son, S. F., Chen, Y., and Guildenbecher, D. R., "Agglomerate Sizing in Aluminized Propellants Using Digital Inline Holography and Traditional Diagnostics," *J. Propul. Power*, Vol. 34, No. 4, 2018, pp. 1002–1014.

[12] Chen, Y., Guildenbecher, D. R., Hoffmeister, K. N. G., and Sojka, P. E., "Digital Imaging Holography and Pyrometry of Aluminum Drop Combustion in Solid Propellant Plumes," *Proceedings of the Imaging and Applied Optics Conference: Laser Applications to Chemical, Security and Environmental Analysis*, 2016. LT4F.2.

[13] Chen, Y., Heyborne, J. D., and Guildenbecher, D. R., "Time-resolved Digital In-line Holography and Pyrometry for Aluminized Solid Rocket Propellants," *Proceedings of the Imaging and Applied Optics Conference: Laser Applications to Chemical, Security and Environmental Analysis*, 2018. LTu3C.5.

[14] Yeager, J. D., Bowden, P. R., Guildenbecher, D. R., and Olles, J. D., "Characterization of Hypervelocity Metal Fragments for Explosive Initiation," *J. Appl. Phys.*, Vol. 122, No. 3, 2017, p. 035901.

[15] Guildenbecher, D. R., Hoffmeister, K. N. G., Kunzler, W. M., Richardson, D. R., and Kearney, S. P., "Phase Conjugate Digital Inline Holography (PCDIH)," *Opt. Lett.*, Vol. 43, No. 4, 2018, pp. 803–806.

[16] Chen, Y., Heyborne, J. D., Guildenbecher, D. R., Smyser, M. E., and Slipchenko, M. N., "Ultra-high-speed Pulse-burst Phase Conjugate Digital In-line Holography for Imaging Through Shock-wave Distortions," *57th AIAA Aerospace Sciences Meeting, AIAA SciTech*, 2019.

[17] Hoffmeister, K. N. G., Kearney, S. P., and Guildenbecher, D. R., "Optical Phase Conjugate Digital Inline Holography for Correcting Aberations in Particle-laden Flames," *54th AIAA Aerospace Sciences Meeting, AIAA SciTech*, 2016. AIAA-2016-1046.

[18] Mann, C. J., Yu, L., Lo, C.-M., and Kim, M. K., "High-resolution Quantitative Phase-contrast Microscopy by Digital Holography," *Opt. Express*, Vol. 12, 2005, pp. 8693–8698.

[19] Han, J.-H., Li, R.-P., Liu, J.-H., Hai, F.-S., and Huang, M.-J., "Two-step Phase Shifting Differential-recording Digital Holographic Microscopy," *Nature Sci. Rep.*, Vol. 7, 2017, p. 1992.

[20] Liu, J.-P., and Poon, T.-C., "Two-step-only Quadrature Phase-shifting Digital Holography," *Opt. Lett.*, Vol. 34, No. 3, 2009, pp. 250–252.

[21] Meng, X. F., Cai, L. Z., Xu, X. F., Yang, X. L., Shen, X. X., Dong, G. Y., and Wang, Y. R., "Two-step Phase-shifting Interferometry and its Application in Image Encryption," *Opt. Lett.*, Vol. 31, No. 10, 2006, pp. 1414–1416.

[22] Awatsuji, Y., Tahara, T., Kaneko, A., Koyama, T., Nishio, K., Ura, S., Kubota, T., and Matoba, O., "Parallel Two-step Phase-shifting Digital Holography," *Appl. Opt.*, Vol. 47, No. 19, 2008, pp. D183–D189.

[23] Kakue, T., Yonesaka, R., Tahara, T., Awatsuji, Y., Nishio, K., Ura, S., Kubota, T., and Matoba, O., "High-speed Phase Imaging by Parallel Phase-shifting Digital Holography," *Opt. Lett.*, Vol. 36, 2011, pp. 4131–4133.

[24] Tahara, T., Ito, K., Fujii, M., Kakue, T., Shimozato, Y., Awatsuji, Y., Nishio, K., Ura, S., Kubota, T., and Matoba, O., "Experimental Demonstration of Parallel Two-step Phase-shifting Digital Holography," *Opt. Express*, Vol. 18, No. 18, 2010, pp. 18975–18980.

[25] Tahara, T., Ito, K., Kakue, T., Fujii, M., Shimozato, Y., Awatsuji, Y., Nishio, K., Ura, S., Kubota, T., and Matoba, O., "Parallel Phase-shifting Digital Holographic Microscopy," *Bio. Opt. Express*, Vol. 1, No. 2, 2010, pp. 610–616.

[26] Abdelsalam, D. G., Yao, B., Gao, P., Min, J., and Guo, R., "Single-shot Parallel Four-step Phase Shifting using On-axis Fizeau Interferometry," *Appl. Opt.*, Vol. 51, No. 20, 2012, pp. 4891–4895.

[27] Gao, P., Yao, B., Harder, I., Min, J., Guo, R., Zheng, J., and Ye, T., "Parallel Two-step Phase-shifting Digital Holograph Microscopy based on a Grating Pair," *J. Opt. Soc. Am. A*, Vol. 28, No. 3, 2011, pp. 434–440.

[28] Hossein, S., Yaghoubi, S., Ebrahimi, S., Dashtdar, M., Doblas, A., and Javidi, B., "Common-path, Single-shot Phase-shifting Digital Holographic Microscopy using a Ronchi Ruling," *Appl. Phys. Lett.*, Vol. 114, 2019, p. 183701.

[29] Nomura, T., Murata, S., Nitanai, E., and Numata, T., "Phase-shifting Digital Holography with a Phase Difference Between Orthogonal Polarizations," *Appl. Opt.*, Vol. 45, No. 20, 2006, pp. 4873–4877.

[30] Novak, M., Millerd, J., Brock, N., North-Morris, M., Hayes, J., and Wyant, J., "Analysis of a Micropolarizer Array-based Simultaneous Phase-shifting Interferometer," *Appl. Opt.*, Vol. 44, No. 52, 2005, pp. 6861–6868.

[31] Chen, G. L., Lin, C. Y., Yau, H. F., Kuo, M. K., and Chang, C. C., "Wavefront Reconstruction without Twin-image Blurring by Two Arbitrary Step Digital Holograms," *Opt. Exp.*, Vol. 15, No. 18, 2007, pp. 11601–11607.

[32] Ferrari, J., Garbusi, E., and Frins, E. M., "Phase Modulation by Polarization Recording in Bacteriorhodopsin: Application to Phase-shifting Interferometry," *Opt. Lett.*, Vol. 29, No. 10, 2004, pp. 1138–1140.

[33] Micó, V., Zalevsky, Z., Ferreiera, C., and García, J., "Superresolution Digital Holographic Microscopy for Three-dimensional Samples," *Opt. Exp.*, Vol. 16, No. 23, 2008, pp. 19260–19270.

[34] Cuche, E., Marquet, P., and Depeursinge, C., "Spatial Filtering for Zero-order and Twin-image Elimination in Digital Off-axis Holography," *Appl. Opt.*, Vol. 39, No. 23, 2000, pp. 4070–4075.

[35] Shaked, N. T., Zhu, Y., Rinehart, M. T., and Wax, A., "Two-step-only Phase-shifting Interferometry with Optimized Detector Bandwidth for Microscopy of Live Cells," *Opt. Exp.*, Vol. 17, No. 18, 2009, pp. 15585–15591.

[36] Zhang, Y., L u, Q., and Ge, B., "Elimination of Zero-order Diffraction in Digital Off-axis Holography," *Opt. Comm.*, Vol. 240, 2004, pp. 261–267.

[37] Sánchez-Ortiga, E., Ferraro, P., Martínez-Corral, M., Saavedra, G., and Doblas, A., "Digital Holographic Microscopy with Pure-optical Spherical Phase Compensation," *J. Opt. Soc. Am.*, Vol. 28, 2011, pp. 1410–1417.

[38] Latychevskaia, T., and Fink, H.-W., "Practical Algorithms for Simulation and Reconstruction of Digital In-line Holograms," *Appl. Opt.*, Vol. 54, No. 9, 2015, pp. 2424–2434.

[39] Guildenbecher, D. R., Gao, J., Reu, P. L., and Chen, J., "Digital Holography Simulations and Experiments to Quantify the Accuracy of 3D Particle Location and 2D Sizing Using a Proposed Hybrid Method," *Appl. Opt.*, Vol. 52, No. 16, 2013, pp. 3790–3801.

[40] Chen, Y., and Guildenbecher, D. R., "Quantitative, Bias-Corrected Measurements of Droplet Position, Size and Velocity with Digital In-line Holography," *ILASS Americas 29th Annual Conference on Liquid Atomization and Spray Systems*, 2017.

[41] Falgout, Z., Chen, Y., and Guildenbecher, D. R., "Improving the Spatial Dynamic Range of Digital Inline Particle Holography," *Appl. Opt.*, Vol. 58, No. 5, 2019, pp. A65–A73.

[42] Falgout, Z., Chen, Y., and Guildenbecher, D. R., "Improving the Detectable Particle Size Floor of Digital In-line Holography," *14th International Conference on Liquid Atomization and Spray Systems (ICLASS)*, 2018.

[43] Guildenbecher, D. R., Gao, J., Chen, J., and Sojka, P. E., "Characterization of Drop Aerodynamic Fragmentation in the Bag and Sheet-thinning Regimes by Crossed-beam, Two-view, Digital in-line Holography," *Int. J. Multiphase Flow*, Vol. 94, 2017, pp. 107–122.